

Short Communication

Welding input effect on the corrosion behavior and microstructure of heat treated GTAW welds of Inconel 718

M.L. Hernández-Rodríguez¹, M. J. Soria-Aguilar², J.L. Acevedo-Dávila³, R.R. Ambriz-Rojas⁴, F. F. Curiel-López^{5,*}

¹ Universidad Autónoma de Coahuila, Facultad de Ciencias Químicas, Blvd. V. Carranza y José Cárdenas Valdés, C.P. 25280, Saltillo, Coah. México.

² Universidad Autónoma de Coahuila, Facultad de Metalurgia, Carretera 57, Km 5, C.P. 25710, Monclova, Coahuila, México.

³ Corporación Mexicana de Investigación en Materiales SA de CV, Ciencia y Tecnología No. 790, Fracc. Saltillo 400, Saltillo, Coahuila, C.P. 25290, México.

⁴ Instituto Politécnico Nacional CIITEC-IPN, Cerrada de Cecati S/N, Col. Sta. Catarina, C.P. 02250 Azcapotzalco, Ciudad de México, México.

⁵ Instituto de Investigación en Metalurgia y Materiales, Universidad Michoacana de San Nicolás de Hidalgo, A.P. 888, CP 58000, Morelia, Michoacán, México.

*E mail: franciscoel7@yahoo.com.mx

Received: 1 January 2019 / Accepted: 1 March 2019 / Published: 10 April 2019

The susceptibility to corrosion of Inconel 718 weldments after double aging heat treatment was studied by the use of potentiodynamic tests. Plates of 3 mm thick were homogenized at 1080 °C during 1 hour and air cooled, then subjected to a solution process at 980 °C during 1 hour and air cooled. The double aging heat treatment was; (1) aging at 720 °C during 8h and oven cooled at 55 °C/h, and (2) aging at 620 °C during 8h and air cooled at room temperature. After heat treatment, the plates were welded by using gas tungsten arc welding process with low and high heat input. The base metal (BM) and the weldments were analyzed by optical microscopy (OM), scanning electron microscopy (SEM) and X-Ray diffraction (XRD). The potentiodynamic tests were carried out in a 3.5% NaCl for the welded samples. The results show that, as the heat input increases, the corrosion rate increases in the weldments. This behavior can be attributed to the microsegregation of Nb and Mo, resulting in a Fe dilution into the weld pool.

Keywords: Inconel 718, corrosion, heat input, double aging, GTAW

1. INTRODUCTION

Nickel base alloys have been extensively used for decades due to their attractive properties of corrosion resistance and stable behavior at high temperatures, because of this, they are used in a wide

variety of applications such as naval industry, aerial industry and power generation [1-4]. Inconel 718 is strengthened by the precipitation of γ' (Ni_3Nb) and MC-carbides mainly, resulting in creep resistance and high strength at high temperatures during long term exposure [5].

The high resistance at elevated temperatures of Inconel 718 is mainly due to the precipitation and distribution of the γ'' phase, it is greatly advisable to use heat treatments in order to increase the mechanical properties due to the precipitation of the γ'' phase in the matrix [6]. Usually, the Inconel 718 alloy is subjected to two subsequent heat treatments to raise its mechanical properties, solubilization between 1021 and 1052 °C for 1-2 1/2 h followed by cooling in air, and aging at temperatures between 774 and 802 °C maintaining the temperature for 6-8 h followed by a cooling in air at a fast speed [7]. Nonetheless, due to the processing of this alloy, it is common the presence of secondary phases such as δ , σ , Laves and MC-type carbides, which can lead to untimely failure when the component is exposed in service. This problem can be aggravated if fusion welding processes are used, where the heat input can cause the growth and formation of such phases [8].

For this, heat treatments of homogenization, solubilization and aging have been used with the purpose of dissolving the phases and carbides in the matrix of the Inconel 718 microstructure. On the other hand, the use of double aging guarantees the formation of the phases γ' and γ'' , where, γ'' is a disc-type more stable phase [9].

In this work, a study of the corrosion behavior on the Inconel 718 and welded joints in a heat treatment of homogenization, solubilization and double aging condition was carried out. Two different heat input were studied in a 3.5% NaCl solution at room temperature.

2. EXPERIMENTAL PROCEDURE

2.1 Heat treatment of base metal

The chemical composition of the Inconel 718 used in this research is shown in Table 1. The base metal (BM) was studied in the annealed condition, where some traces of Nb, Ti and Al were present as well as MC carbides. Samples of 3mm thick were prepared mechanically to obtain a single V bevel. After machining, the plates were subjected to heat treatment before welding; first, the plates were homogenized at 1080 °C during 1 h and then air cooled, after that, the samples were subjected to a solution treatment at 980 °C during 1 h and later air cooled. For the precipitation process, a double aging heat treatment was carried out in the specimens; (1) aged at 720 °C during 8h and oven cooled at 55 °C/h, subsequently (2) aged at 620 °C during 8h and air cooled at room temperature. Figure 1 shows the heat treatment cycle performed in the Inconel 718.

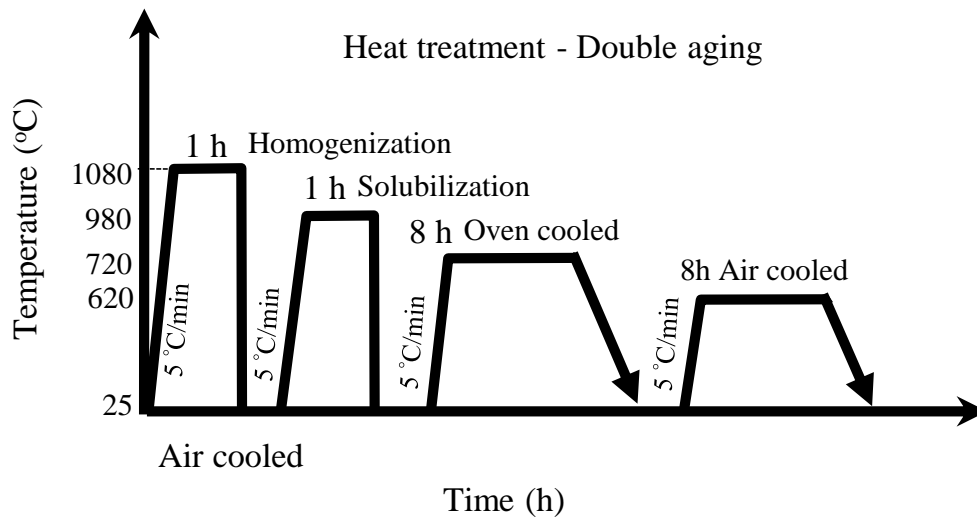


Figure 1. Heat treatment cycle performed in the samples of Inconel 718.

Table 1. Chemical composition of Inconel 718.

	Elements (% wt)													
	C	Si	Mn	P	S	Cr	Mo	Al	Cu	Ti	Fe	Co	Nb	Ni
Nominal	0.080	0.35	0.35	0.015	0.015	21	3.3	0.80	0.03	1.15	17	1.0	5.5	Bal.
Base metal	0.03	0.06	0.07	0.008	0.001	18.64	2.85	0.55	0.10	0.93	17.84	0.24	4.84	Bal.

2.2 Welding process

After the double aging heat treatment, the plates were welded by using a gas tungsten arc welding process (GTAW) employing a Miller Dynasty 700 source, and Argon 100% as shielding gas. A filler metal (IN718) was feed externally during the welding. Two samples named as M1 and M2 were welded with two different heat input. The welding parameters are presented in Table 2.

Table 2. Welding parameters for GTAW process.

Sample	M1	M2
Current (A)	270	356
Voltage (V)	27.3	29 V
Flow rate (L/m)	14.15	14.15
Feed rate (cm/min)	482	482
Welding speed (mm/s)	3.6	1.7
Heat input (kJ/mm)	1.229	3.644

2.3 Microstructural characterization

For microstructural characterization, conventional metallography sample preparation was carried out using grinding and polishing in the BM and the weldments. The samples were etched with a mix of HCl, HNO₃, HF and distilled water at room temperature and observed in an optical microscope. The weldments were analyzed in more detail in the fusion line (FL), heat affected zone (HAZ) and parent metal by using a scanning electron microscope equipped with an energy dispersive X-ray (EDX) analyzer.

2.4 X-ray diffraction analysis

X-ray diffraction analysis was performed in the base metal and in samples near to the welding bead. The samples were analyzed in a Panalytical diffractometer equipped with Cu α radiation. During the tests, data were acquired in a 2Θ range from 30° to 100°, pass in $2\Theta = 0.01^\circ$ and time between pass $\phi = 0.1$ min.

2.5 Potentiodynamic polarization tests

Samples of 2 mm in thickness were cut parallel to the weld bead for potentiodynamic polarization tests. The specimens were mounted in resin after attaching a copper wire in the back side of the sample to connect the potentiostat. The samples were prepared prior to the electrochemical tests by grinding with 600 grit emery paper, ultrasonically degreased and cleaned with acetone and dried. The potentiodynamic polarization tests were conducted with a conventional electrochemical cell consisting of a saturated calomel electrode (SCE) as reference electrode, a graphite counter electrode and the samples as a working electrode. The scan rate of the tests was 50 mV/min in a 3.5% NaCl solution in the range of -600 mV to 1300mV vs. the open circuit potential (OCP). All the tests were conducted in a Gill ACM unit at room temperature.

3. RESULTS AND DISCUSSION

3.1 Microstructural analysis of the BM and heat treatment

The Inconel 718 was cut and analyzed transversal, longitudinal and superficially by optical microscopy. Figure 2 shows the micrographs of the BM, where it can be seen austenitic equiaxed grains and the presence of twinning between the grain boundaries due to the thermomechanical process. On the other hand, carbides MC-type (dark spots) are present randomly through the matrix. The grain size measured according to ASTM E-112 corresponds to number 9 with a mean distribution of 3,968 grains/mm² [10]. Nonetheless, in Figure 3 it can be observed a SEM image with an elemental mapping performed on an MC carbides area, where Fe, Nb and Ti (green, yellow and purple, respectively) are main elements inside the analyzed particle. Such carbides are formed after the solidification process, and

they can transform in different stoichiometry carbides, i.e. $M_{23}C_6$, M_6C , M_7C_3 , its presence can contribute to the hardening of this alloy [11].

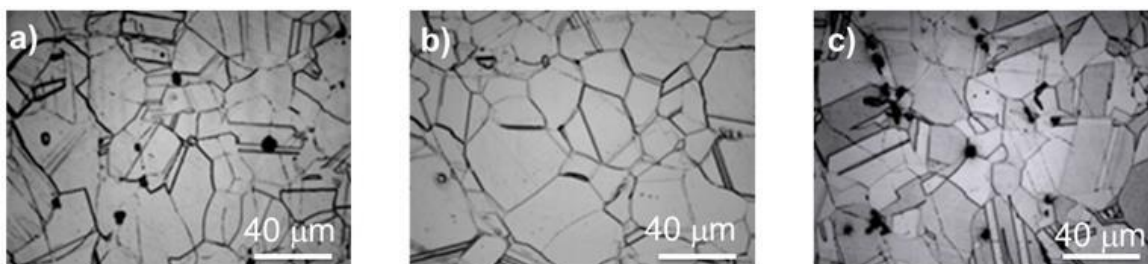


Figure 2. Optical micrographs of Inconel 718. a) transversal 50x, b) longitudinal 50x y c) superficial 50x.

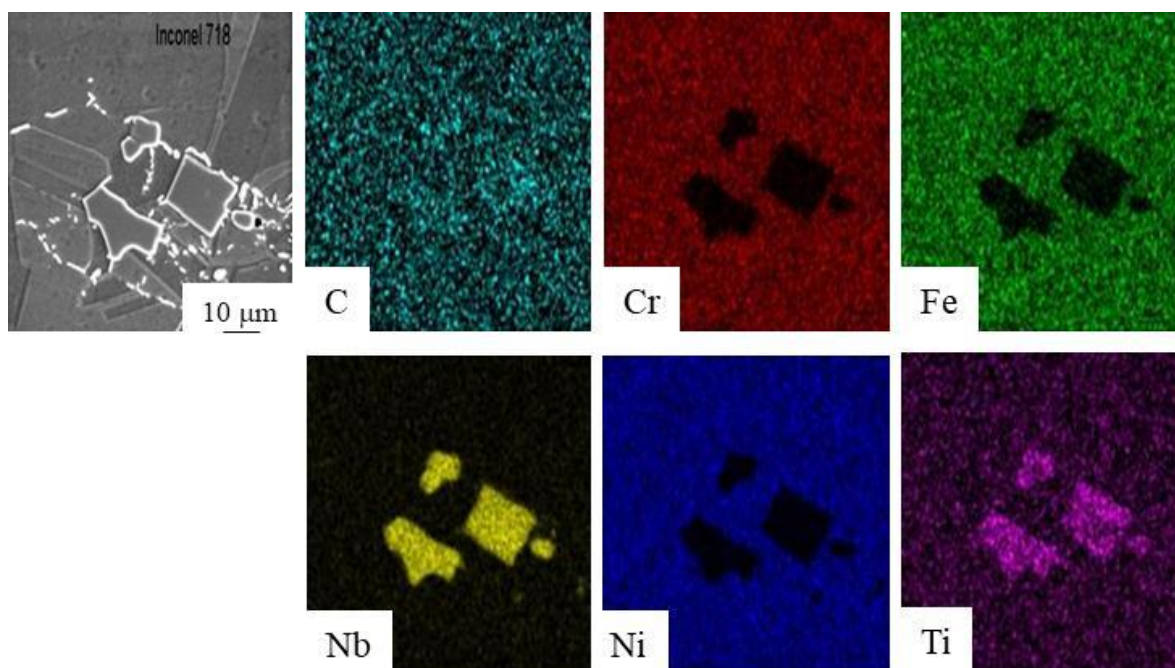


Figure 3. Elemental mapping performed in the BM of Inconel 718.

The heat treatments of Inconel 718 standard and double aging were carried out at high temperatures in the austenite field with the objective of increasing the diffusion process of segregated elements and diminishing the chemical concentration gradients produced during the solidification process. The heat treatment of double aging was conducted to precipitate the different shapes and sizes of the γ' and γ'' phases [12]. Figure 4a shows the optical micrograph of Inconel 718 after the double aging and oven cooled, where it can be seen that the grain size increases at $\sim 32 \mu\text{m}$ and the twinning disappears due to the temperature. This behavior can be attributed to the microstructural evolution of the δ phase at 950°C , where it is well known that the existing δ phase is partially re-distributed resulting in a uniform grain boundary structure. Recrystallization is a thermally activated phenomenon, this means that the speed of the mechanisms that control the formation and movement of the boundaries of newly formed wide angle

grains depending on the annealing temperature [13]. On the other hand, Figure 4b shows a SEM image of a specimen in a different area where it can be appreciated the presence of Laves phase (light gray) intergranular as needle-like structure and δ phase within the grain boundaries.

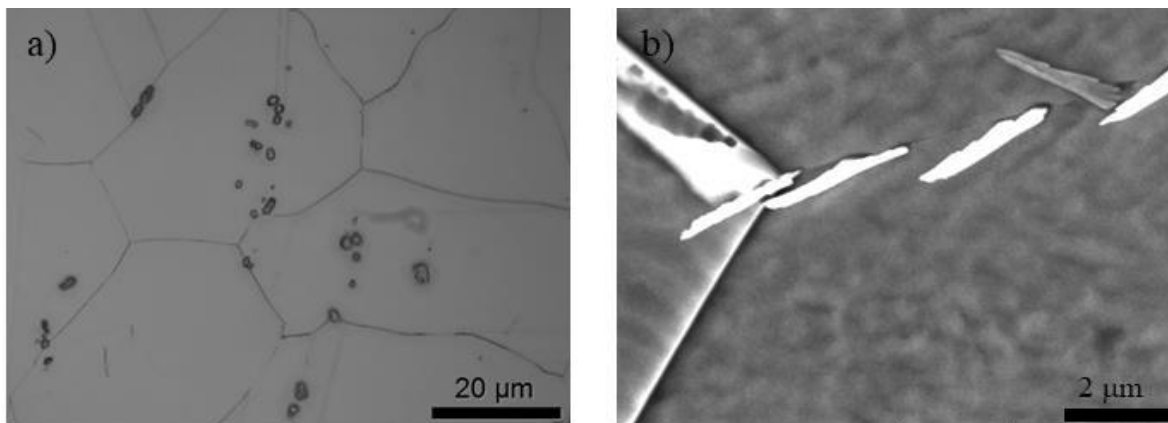


Figure 4. Images of heat treatment of Inconel 718; a) Optical, b) SEM.

3.2 Microstructural analysis of the welds

The microstructural characteristics in the samples with the heat treatment of double aging on the welds performed with the GTAW welding process using two different heat inputs were evaluated in the superalloy Inconel 718. Figures 5a and 6a show the macrographs of the weldments with low (M1-Z1) and high (M2-Z1) heat input, respectively. These figures show different characteristics of the fusion zone and the heat-affected zone (HAZ) of the welds. Figure 5b shows a micrograph of the pool zone of the welds where, it can be seen fine equiaxed dendrite structures. The transformation of coarse columnar dendrites to fine equiaxed dendrites is due to the higher cooling rate reached in the welding process during cooling [14]. The particles dispersed (dark) inside of the dendrites appear in a chain-like structure, where the analysis performed in more detail shows that such particles correspond to the Laves phase. In Figure 5c an island of Laves phase was analyzed and the Table 3 show the chemical composition. On the other hand, a carbide is present near the border between the matrix and the Laves phase. The chemical analysis of this Ni-rich particle matches well with a Nb-rich carbide [15]. The chemical composition is the same for both heat inputs used in this study.

Figure 6b shows the microstructure of the sample welded with the highest heat input, where it can be seen that, the presence of the Laves phase is higher compared to the sample welded with less heat input. Such phase is segregated between the dendritic spacing of the melted zone.

It is well known that microsegregation of elemental constituents occur during the solidification process in a welded joint, where elements such as Mo, Nb, and Ti segregate between the dendrites and other elements i.e. W, Fe, Cr, and Co segregate into the core regions. The formation of the Laves phase and Nb-rich carbides is the consequence of the solidification phenomena in the melted zone of the weld [16]. In this case, the slow cooling rate due to the greater heat input could be the driving force to induce

the segregation and formation of the Laves phase, this assumption is because its formation is controlled by a diffusion process.

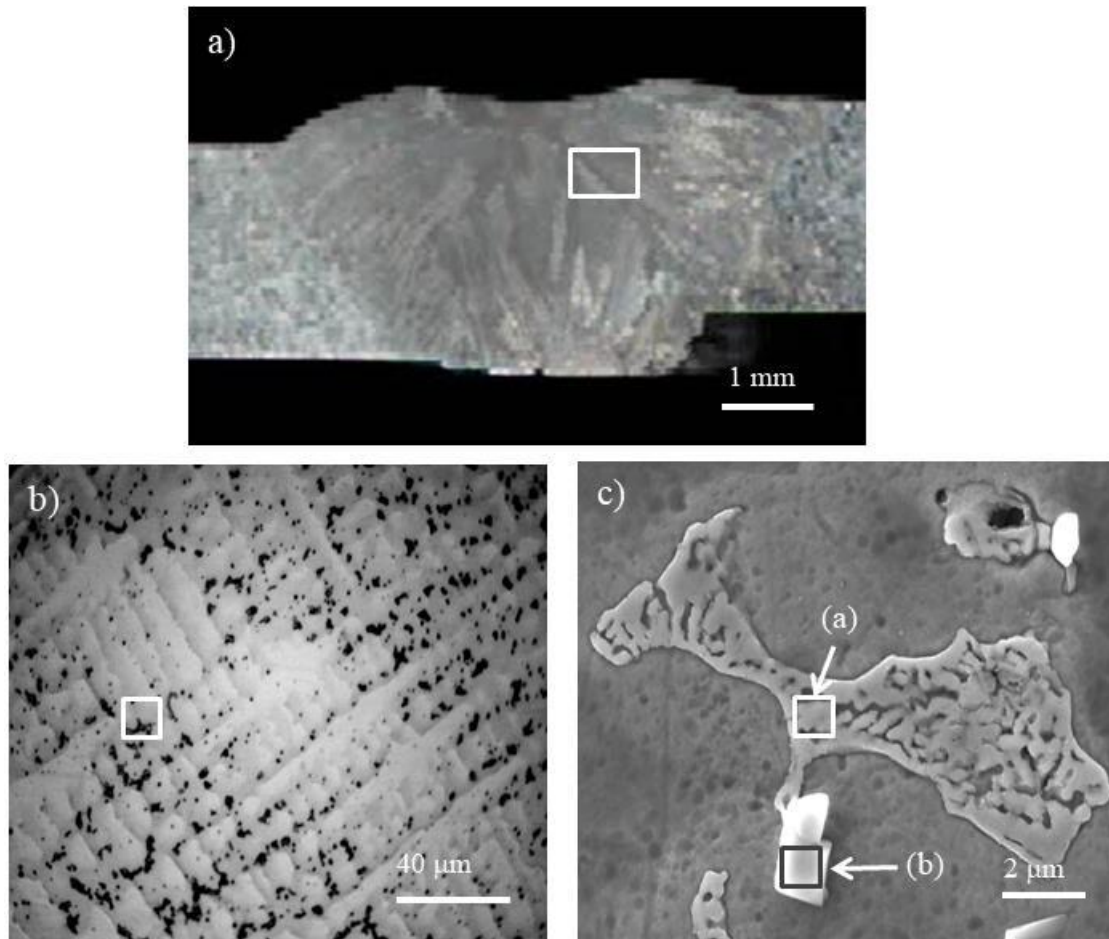


Figure 5. Weld of Inconel 718 with low heat input, a)macro, b) weld pool, c) analyzed particle.

In the Inconel 718 alloy, the γ'' phase (Ni_3Nb), can be replaced by the Laves phase due to the presence of Fe, Cr, Ti, and Nb as shown in Table 4. The Laves phase is an intermetallic compound, for example in a binary alloy system, its structure type is A_2B , where $A = Fe, Ni, Cr$ and $B = Nb, Mo, Si, Ti, Zr, Hf, \text{ and } Ta$ [17]. The precipitation of the Laves phase (Fe_2Nb) is effective to the strengthen grain boundaries and suppress deformation, improving creep resistance [18].

Table 3. Chemical composition of weld of low heat input.

Chemical composition						
Location	Ti	Cr	Fe	Ni	Nb	Tl
(a)	2.18	23.48	15.24	29.57	21.26	8.27
(b)	11.79	6.82	7.37	19.40	49.78	4.83

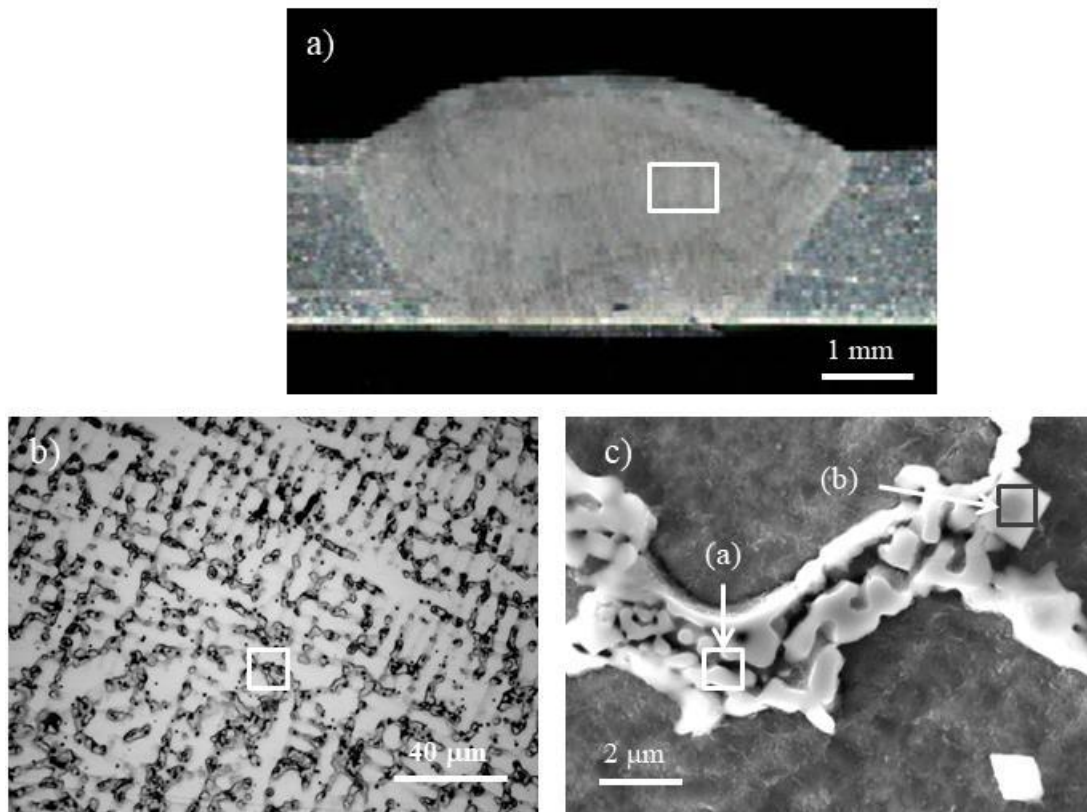


Figure 6. Weld of Inconel 718 with high heat input, a)macro, b) weld pool, c) analyzed particle.

Table 4. Chemical composition of weld of high heat input.

Location	Chemical composition (wt %)											
	C	O	Al	Si	Ti	Cr	Fe	Ni	Nb	Mo	Ta	Tl
(a)	6.88	2.47	0.03	0.31	0.95	11.8	12.5	35.1	25.7	3.16	-	-
(b)	12.04	-	0.26	-	16.6	4.13	3.64	9.0	53.9	-	0.19	0.18

3.3. X-ray diffraction analysis

X-ray diffraction analysis was carried out in the base material (BM) of Inconel 718 under the as-received condition and in a sample subjected to the heat treatment (HT) of double aging, as well as the samples of the welds performed with low heat input (M1), and high heat input (M2). Figure 7 shows the X-ray diffraction patterns where it can be seen the presence of the γ' and/or γ'' phases, carbides MC-type and δ phase (Ni_3Nb), the two hardening phases were detected in the specimens. Concerning the results of the chemical composition of MC-type carbides, the microanalysis of X-ray scattering energy reported above suggests that MC-type carbides are a combination of Nb and Ti [19].

Nonetheless a new peak of the orthorhombic δ phase appears in the thermal double ageing heat treatment, the same occurs for the samples welded with low and high heat input. These results correspond

to the previous observations, where the amount of δ phase precipitates in the interior of the grains and in the grain boundary after the aforementioned thermal treatments; the basic difference in the structures γ'' -Ni₃Nb and δ -Ni₃Nb lies in the stacking sequence of the compact packing planes; in the crystal structure bct (D0₂₂) - the sequence is abcabc, in orthorhombic (D0_a) - the sequence is ababab respectively [20].

On the other hand, the carbides tend to precipitate in the heat treatment and the size of the crystallite decreases as can be seen in Table 5, where, only a few carbide peaks are visible in the XRD pattern. The uniform dispersion of the hardening γ' and γ'' phases are also precipitated in the austenitic matrix due to the heat treatment of aged the double aging, however, it is not evident to distinguish the XRD peaks of the γ' and γ'' phases from the matrix phase γ due the overlap of the peaks [21].

In the patterns of the samples welded with low heat input (M1-Z1) and with high heat input (M2-Z1), the presence of δ phase as well as γ'' can be appreciated. It is reasonably to establish that the absence of diffraction peaks of type MC carbides in the diffraction patterns of the samples welded with high and low contribution may be due to the reduced size and/or quantity of MC particles [22].

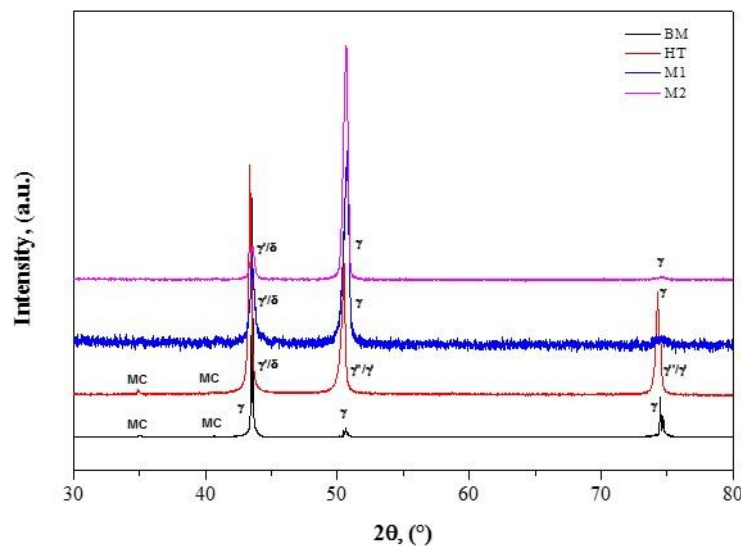


Figure 7. X ray diffraction analysis of the base metal, heat treatment and welds of Inconel 718.

Table 5. Results of the crystallite size and micro-tension of the samples studied by X ray diffraction.

	Identification	Cauchy method	
		ZC	MD
Base metal	MB	19.53	0.00561124
Heat treatment	HT	4.38	0.05895654
Weld with low heat input	M1-Z1	7.53	0.01162748
Weld with high heat input	M2-Z2	4.57	0.01775024

The Cauchy method was used to determine the crystallite size (CZ) and the micro-strains in this study; this method considers that the widening of the profile is mainly due to the crystallite defects, although the effects of micro-tension are also considered.

In the results, the tendency of the heat treated sample to decrease the size of the crystallite as well as the increase of the among of micro-strain was observed; since the micro-strains are a measure of the residual voltage present in the atomic lattice, are produced by the strain process or the thermal treatment, as is the case of the sample analyzed.

In the samples welded with low and high heat input, it can be appreciated that the micro-strains decrease in comparison with the sample thermally aged. The measurement of the crystallite indicates that as the heat input increases, there are smaller changes of the values of the size of the crystallite.

3.4. Corrosion resistance test

In order to evaluate the corrosion behavior of the samples subjected to the heat treatment of double aging and subsequent welding process, potentiodynamic polarization test was performed on samples cut from each welding with low heat input (M1) and high heat input (M2) to be evaluated at 25 °C in a 3.5% NaCl solution. Figure 8 shows the polarization curves performed in the fusion zone of the weld made with low heat input (M1-Z1) and high heat input (M2-Z1). The cathodic loop in the curves show evolution of hydrogen gas reaction in both cases. On the other hand, the anodic loop shows and active behavior in the alloy, where the pitting potential reached for the weld made with low heat input was 409.1 mV and 340.8mV for the high heat input. The value of the current density (I_{corr}) for the samples welded with low heat input was $0.0277E^{-6}$ A/cm² and higher values of current density as $0.165E^{-6}$ A/cm² were observed for the samples welded with high heat input. The data obtained from the polarization curves can be observed in Table 6. From this study it is evident that as the heat input increases, the current density increases almost by one decade, reducing the corrosion resistance of the weldments. Guo et al. reported that non-desirable phases segregate during the solidification process in the interdendritic zone of liquid metal produces detrimental corrosion resistance due to the precipitation of intermetallic compounds including Laves phase [23]. On the other hand, Kim et al. reported that as the heat input increases, the corrosion rate elevates its value due to the microsegregation of Nb and Mo, resulting in a Fe dilution into the weld pool [24]. Such behavior was observed in our study, where it is appreciated that greater heat input promotes a higher corrosion rate. However, this behavior could be affected depending on the welding process that is being used to join the Inconel 718.

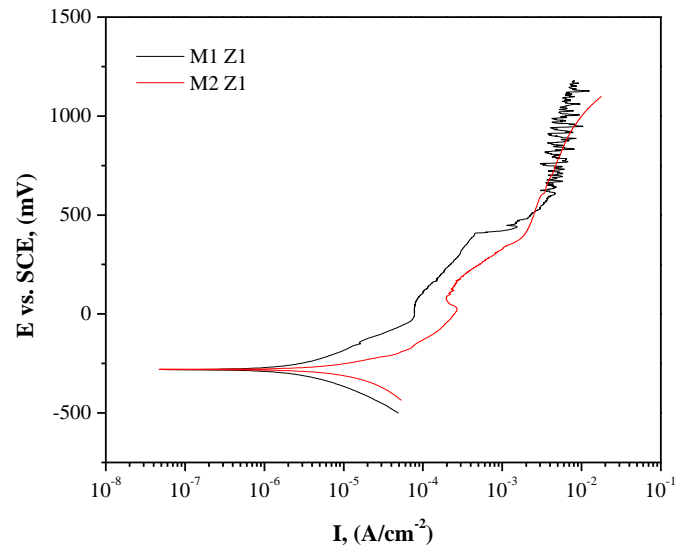


Figure 8. Potentiodynamic polarization; M1 low heat input, M2 high heat input.

Table 6. Experimental values obtained from polarization test in 3.5% NaCl.

Sample	Corrosion potential E_{corr} (mV)	Pitting potential E_{pit} (mV)	ΔE	Corrosion current I_{corr} (A/cm^2)
M1-Z1	-281.30	409.1	960.4	0.0277E^{-6}
M2-Z1	-278.70	340.8	619.5	0.165E^{-6}

4. CONCLUSIONS

From the study carried out on the effect of the double aged thermal treatment on the corrosion behavior of welded joints by the GTAW welding process in Inconel 718, the following conclusions are derived:

1.- In the heat treatment for the double aging of Inconel 718 alloy, the homogenized temperature is high enough, allowing the dissolution of the interdendritic Laves phase and delta phase, which promotes the growing of the average grain size to 32 μm .

2.- The transformation of coarse columnar dendrites to fine equiaxed dendrites is due to the higher cooling rate reached in the welding process during cooling.

3.- In the corrosion tests, as the heat input increases by the welding process, the current density increases almost by one decade, increasing the corrosion rate of the weldments. This can be attributed to the microsegregation of Nb and Mo, resulting in a Fe dilution into the weld pool. However, this behavior could also be affected depending on the welding process that is being used to join the Inconel 718.

ACKNOWLEDGEMENTS

The authors want to thank to CONACyT for the financial support for this PhD project.

References

1. K.D. Ramkumar, S. Dev, K.V. Phani, R. Rajendran, K.G. Mugundan, and S. Narayanan, *Journal of Materials Processing Technology*, 266 (2019) 52.
2. A.H. Musfirah, J.A. Ghani, C.H. and C. Haron, *Wear*, 376-377 (2017) 125.
3. M.J. Donachie and S.J. Donachie, *Superalloys: A Technical Guide*, 2nd Edition, ASM International, 2002.
4. M. Durand-Charre, *The microstructure of superalloys*, 1st ed., Routledge, London, 2017.
5. J.W. Han, S.H. Jung, H. Cho and H.W. Lee, *International Journal of Electrochemical Science*, 13 (2018) 2829.
6. N.E. Bagourty, M.A. Amin and Q. Mohsen, *International Journal of Electrochemical Science*, 6 (2011) 6718.
7. D. Pereira, T. Clarke, R. Menezes and T. Hirsch, *Materials Science and Technology*, 31 (2015) 669.
8. K.C.G. Candioto, F.R. Caliari, D.A.P. Reis, A.A. Couto and C.A. Nunes, *Characterization of the Superalloy Inconel 718 After Double Aging Heat Treatment*, in: C. Springer (Ed.) *Mechanical and Materials Engineering of Modern Structure and Component Design*, 2015.
9. C. Wang, R. Li, *Journal of Materials Science*, 39 (2004) 2593.
10. ASTM E112-13. *Standard Test Methods for Determining Average Grain Size*.
11. B. Geddes, H. Leon and X. Huang, *Superalloys: Alloying and Performance*, ASM International, 2010.
12. D. Zhang, W. Niu, X. Cao and Z. Liu, *Materials Science and Engineering: A*, 644 (2015) 32.
13. P. Páramo-Kañetas, U. Öztürk, J. Calvo, J.M. Cabrera and M. Guerrero-Mata, *Journal of Materials Processing Technology*, 255 (2018) 204.
14. S.G.K. Manikandan, D. Sivakumar, K.P. Rao and M. Kamaraj, *Journal of Materials Processing Technology*, 214 (2014) 358.
15. G. Asala, J. Andersson and O.A. Ojo, *The International Journal of Advanced Manufacturing Technology*, 87 (2016) 2721.
16. A.V. Reddy, K.P. Rao and G.M. Reddy, *Materials Science and Technology*, 21 (2005) 1132.
17. K.S. Kumar and P.M. Hazzledine, *Intermetallics*, 12 (2004) 763.
18. S.W. Chen, C. Zhang, Z.X. Xia, H. Ishikawa and Z.G. Yang, *Materials Science and Engineering: A*, 616 (2014) 183.
19. C. Slama, C. Servant and G. Cizeron, *Journal of Materials Research*, 12 (2011) 2298.
20. M. Sundararaman, P. Mukhopadhyay and S. Banerjee, *Acta Metallurgica*, 36 (1988) 847.
21. S.-H. Zhang, H.-Y. Zhang and M. Cheng, *Materials Science and Engineering: A*, 528 (2011) 6253.
22. Y. Mei, Y. Liu, C. Liu, C. Li, L. Yu, Q. Guo and H. Li, *Materials & Design*, 89 (2016) 964.
23. Q. Guo, Y. Li, J. Qian, H. Yu and C. Chen, *International Journal of Electrochemical Science*, 12 (2017) 8929.
24. J. Suk and H. Woo, *International Journal of Electrochemical Science*, 10 (2015) 6454.